Comparison of Design Techniques for Pumps with Skewed Blades

A. L. Treaster* and F. E. Smith*
Pennsylvania State University, State College, Pennsylvania

Two different approaches, developed over a period of approximately 12 years, of including blade skew effects in the design of a pump rotor are presented. Performance comparisons are included between the radial and skewed bladed rotor for each of the pump designs. The streamline curvature method which incorporated skew effects and secondary flow losses produced a skewed rotor that satisfactorily met the design performance goals, whereas a design procedure using a bound vorticity approach did not.

Nomenclature

A_R = πR_R^2 = rotor disk area, ft^2
$C_{\dot{m}}$ = mass flowrate/$\rho A_R V_\infty$ = dimensionless mass flowrate coefficient
D_R = diameter of rotor, ft
F_R = radial component of the body force per unit mass, lb/slug
g = gravitational constant = 32.2 ft/s^2
h = height in flow passage above hub reference, ft
h_T = total blade span, ft
H = fluid head rise across the rotor, ft
J = $V_\infty / n D_R$ = advance ratio, dimensionless
K_Q = $Q/\frac{1}{2}\rho n^2 A_R D_R^3$ = dimensionless torque coefficient
k = computational pass number in the streamline curvature method
l = projected blade chord length in streamwise direction, ft
M = meridional or streamwise direction
n = rotor speed, rev/s
N = number of blades
P = local fluid static pressure, lb/ft^2
P_T = local fluid total pressure, lb/ft^2
P_V = vapor pressure of fluid at bulk temperature T, lb/ft^2
Q = rotor torque, lb·ft
R = radial coordinate, ft
R_C = local radius of curvature of a meridional streamline, ft
R_H = hub radius, ft
R_R = rotor tip radius, ft
$\bar{R}$ = mean flow radius, ft
U = rotor rotational speed, ft/s
u,v = induced velocity component in x and y directions, ft/s
V_θ = circumferential velocity component, ft/s
V_M = meridional velocity, ft/s
V_{M_i} = induced meridional velocity, ft/s
V_∞ = freestream velocity, ft/s
x,y = Cartesian coordinates with the origin at the blade mid-chord, midspan point, ft
Z = axial coordinate in cylindrical coordinate system measured from computing station 1, ft
z = $x+iy$ = complex number, ft
Γ = circulation, ft^2/s
Γ_θ = circulation corresponding to ξ_θ, ft^2/s
η = dimensionless relaxation factor
λ = dimensionless effective area coefficient
θ = circumferential angular coordinate, rad
θ_P = peripheral angular coordinate of the blade pressure surface, rad
θ_S = peripheral angular coordinate of the blade suction surface, rad
ξ_R = radial component of vorticity, s^{-1}
ξ_θ = circumferential component of vorticity, s^{-1}
ρ = fluid density, slugs/ft^3
ϕ = local inclination angle of the meridional streamlines with respect to the pump centerline, rad
ψ = skew angle, rad
ω = complex velocity potential, ft^2/s

Presented as Paper 83-1282 at the AIAA/SAE/ASME 19th Joint Propulsion Conference, Seattle, Wash., June 27-29, 1983; received Oct. 12, 1983; revision received Sept. 21, 1984.

*Research Associate, Applied Research Laboratory.

Introduction

TWO different approaches of including blade skew effects in the design of a pump rotor are presented. The second approach reflects approximately 12 years of technological development of computational techniques and a greater understanding of the details of the flow through a turbomachine than was available at the time of the first design.

In this paper, the turbomachinery term "skew" is defined as the departure of the blade stack-up line or a bound vortex line representing the blade from a radial line in the R, θ plane. The geometrical relationships are shown in Fig. 1, where the local skew angle ψ is defined as the angle between the tangent to the stack-up line and a radial line through the tangency point. Skewed blades are used in turbomachines and pumps because of their favorable interaction with spatially distorted inflows which reduces unsteady forces. In pumps these distorted inflows at the rotor inlet plane can be caused by upstream support struts.

Different programs to improve pump design procedures have been conducted. In these programs attempts are made to include new and more accurate design methods and to evaluate the resulting pump hardware experimentally. Two of these pump design programs, conducted approximately a decade apart in time, are discussed to illustrate the evolution of the design procedures, particularly with respect to blade skew and energy losses.

In the early 1960's, a bound vorticity approach was used to model the induced effects of skewing on the rotor blade design. Using this design technique, a skewed bladed rotor (design I) was designed and fabricated to replace a conventional radial bladed rotor in a pump. After tests were run and the performance of the two rotor configurations compared, the skewed rotor design was found to be less than satisfactory. The skewed rotor's power requirements were higher than desired and the cavitation resistance did not meet the design goals.

In the latter half of the 1970's, a second pump unit was designed (design II). Here again, both a radial bladed rotor and a skewed bladed rotor were designed for the pump. The design procedure used for this pump application was the streamline curvature method (SCM), in which the effects of blade skew and inlet and secondary flow losses were incorporated. The resulting pump hardware was experimentally evaluated. The performance of the skewed bladed rotor was found to be better than the radial rotor and met the design performance goals.

Subsequently, the SCM design approach was reapplied to the first skewed rotor (design I). The comparison of these two rotor design methods applied to the design I skewed rotor partially explains the performance deficiencies observed with the design I rotor. These two pump design approaches and the experimental evaluations are discussed in the remainder of this paper.

Original Design Procedure

Development of the design procedure for a skewed bladed pump rotor was initiated in response to the need for reduced vibration in a radial pump system. The pump, shown schematically in Fig. 2, had a rotor operating in a spatially nonuniform inflow. Because the flowfield contained strong circumferentially spaced wakes produced by the upstream casing support struts, skewed blading on the rotor was desired to reduce the unsteady force interactions between the rotor blading and these wakes.

In design I, the inlet and exit plane radial distributions of meridional velocity were derived from experimental data coupled with radial equilibrium considerations. Knowledge of the radial rotor design parameters permitted specification of the mass flow rate coefficient $C_{\dot{m}}$, the rotor head rise $H/(V_\infty^2/2g)$, and the required rotor exit plane distribution of circumferential velocity V_θ/V_∞ across the duct. The rotor design problem then became one of approximating the effect of the skewed rotor blades on the "unskewed" meridional velocity profiles.

To approximate the skew effects, the rotor blade was represented by the skewed bound vortex line shown in Fig. 1. The circumferential component of this bound vortex induces velocities in the meridional plane that must be accounted for. The circulation Γ and vorticity components ξ_R and ξ_θ for a blade $\ell \times h_T$ in planform shape (see Fig. 2) were approximated at the radii that divided the flow area in half, $\bar{R}$. Thus the circulation around the rotor and the associated vorticity were calculated from

$$\Gamma = 2\pi \bar{R} V_\theta \tag{1}$$

and

$$\xi_R = \Gamma / 2\pi \bar{R} \ell \tag{2}$$

and

$$\xi_\theta = \xi_R \tan\psi \tag{3}$$

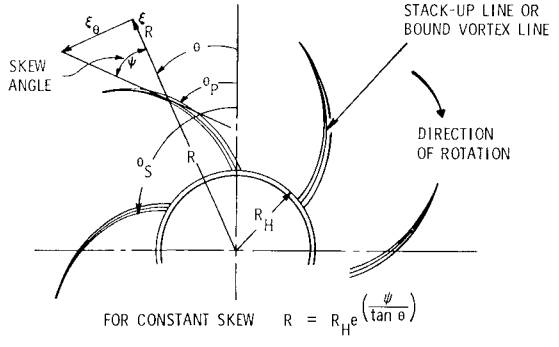

Fig. 1 Definition of skewed blade geometry.

The circulation associated with ξ_θ is

$$\Gamma_\theta = \ell h_T \xi_\theta = h_T V_\theta \tan\psi \tag{4}$$

and can be calculated from the preliminary design parameters. If a ring vortex of this strength had been concentrated at $\bar{R}$, the induced velocities at the rotor inlet and exit planes could easily have been calculated; however, the boundary conditions at the hub and casing would not have been satisfied. Instead, a two-dimensional vortex of strength Γ_θ was assumed at the midchord, midspan point ($x=0.0$, $y=0.0$) of the projected blade planform. To satisfy the wall boundary conditions, a system of image vortices of strength Γ_θ, separated by a distance h_T and alternating in sign were distributed along the y axis. The complex potential for this system is

$$\omega = -(\Gamma_\theta/2\pi)\, \ell n \tanh(\pi z/2h_T) \tag{5}$$

and the induced velocity components can be calculated from

$$u = -\frac{\Gamma_\theta}{2h_T} \frac{\cosh(\pi x/h_T)\sin(\pi y/h_T)}{\sinh^2(\pi x/h_T)+\sin^2(\pi y/h_T)} \tag{6}$$

and

$$v = \frac{\Gamma_\theta}{2h_T} \frac{\sinh(\pi x/h_T)\cos(\pi y/h_T)}{\sinh^2(\pi x/h_T)+\sin^2(\pi y/h_T)} \tag{7}$$

To satisfy the continuity condition, the resulting induced velocity profiles were shifted in the flow direction until their integrated contribution to the mass flow rate was zero. The resulting meridional velocity (V_M/V_∞) profiles are shown in Figs. 3 and 4 for the chosen constant skew angle of $\psi = 40$ deg.

The rotor inlet and exit plane pressure profiles were determined using the continuity and energy equations from the design profiles of V_θ/V_∞ and $H/(V_\infty^2/2g)$, the calculated V_M/V_∞ distributions, and the design advance ratio J.

Once the number of blades was selected (in this case 13), four equally spaced cylindrical blade sections were designed by the mean streamline method of Wislicenus.[1] The complete blade shape was hand-lofted from the four design sections. The resulting skewed bladed rotor is shown in comparison with the radial rotor in Fig. 5.

Experimental Evaluation of Pump Design I

The design I pump was evaluated primarily from a powering and cavitation point of view. The powering data are characterized by the torque coefficient K_Q vs advance ratio J curve shown in Fig. 6. Here the results obtained with a radial rotor designed for the same application are shown for comparison purposes. Over the range of advance ratios tested, K_Q for the skewed rotor is 7-9% higher than that measured with the reference radial rotor operating in the design I pump.

The cavitation characteristics of the design I skewed rotor are shown in Fig. 7. Here again the data measured with the

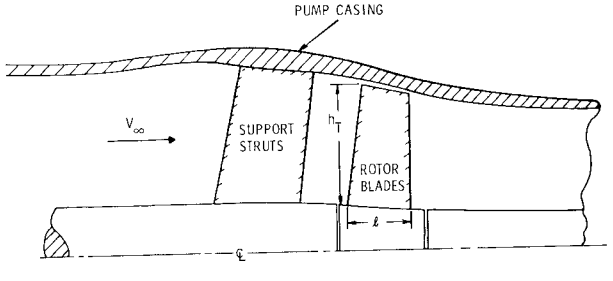

Fig. 2 Typical pump configuration.

skewed rotor are compared with those from the radial rotor. These data indicate that the skewed rotor is more cavitation prone over the major portion of the operating J range. The controlling form of cavitation is leading-edge pressure surface cavitation. This form of cavitation is usually indicative of improper flow incidence angle at the leading edge of the blade. Both the powering requirements and the cavitation characteristics of the design I skewed pump rotor were higher than the acceptable limits of the design goals.

Improved Design Procedure

The availability of high speed digital computers and the implementation of sophisticated curve fitting techniques facilitated the development of the improved design procedure. This design procedure incorporated an updated, computerized axisymmetric version of the streamline curvature method of flowfield computation. This technique is developed from material discussed in Refs. 3, 4, and 8. Only the governing questions and assumptions will be discussed herein.

In cylindrical coordinates the radial equilibrium equation with no skew effects can be written for a fluid particle at some position (R,Z) in an axisymmetric flowfield as (see Fig. 8)

$$\frac{1}{\rho}\frac{\partial P}{\partial R} = \frac{V_\theta^2}{R} + \frac{V_M^2}{R_C}\cos\phi - V_M\frac{\partial V_M}{\partial M}\sin\phi \tag{8}$$

In Eq. (8) the left-hand term is the radial static pressure gradient, the first term on the right is the normal acceleration due to V_θ, the second term is the radial component of the normal acceleration due to V_M, and the final term is the radial component of the tangential acceleration due to V_M. R_C is negative for the example shown in Fig. 8 and would be positive for a concave-down streamline with respect to the centerline. The static pressure P at any point in the flowfield can be expressed using Bernoulli's equation:

$$P = P_T - \tfrac{1}{2}\rho V_M^2 - \tfrac{1}{2}\rho V_\theta^2 - \rho g h \tag{9}$$

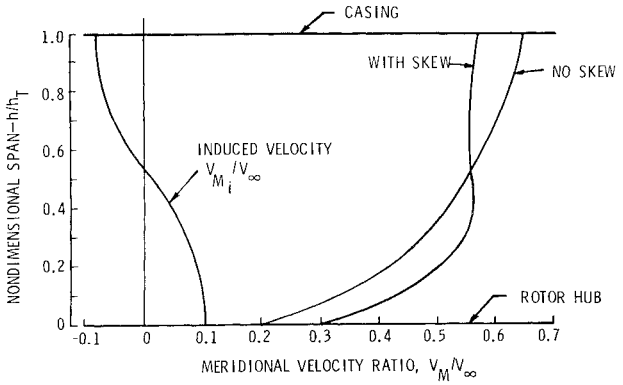

Fig. 3 Design I rotor inlet velocity ratios.

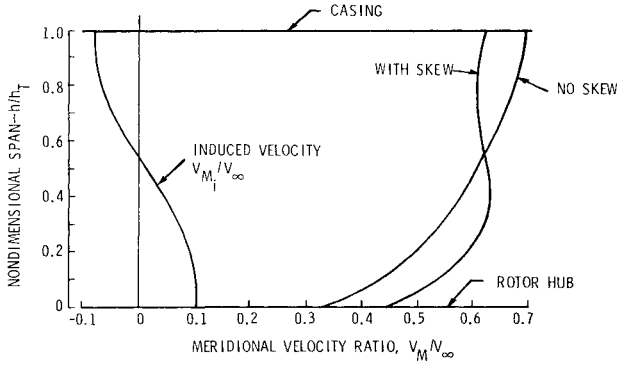

Fig. 4 Design I rotor exit velocity ratios.

When Eq. (9) is differentiated with respect to R and small variations in h are neglected ($\partial h/\partial R \cong 0.0$) the results can be introduced in Eq. (8) to yield

$$\frac{\partial V_M}{\partial R} = \left[\frac{1}{\rho}\frac{\partial P_T}{\partial R} - \frac{V_\theta}{R}\frac{\partial (RV_\theta)}{\partial R}\right]\frac{1}{V_M} - \left[\frac{\cos\phi}{R_C} - \frac{\sin\phi}{V_M}\frac{\partial V_M}{\partial M}\right]V_M \tag{10}$$

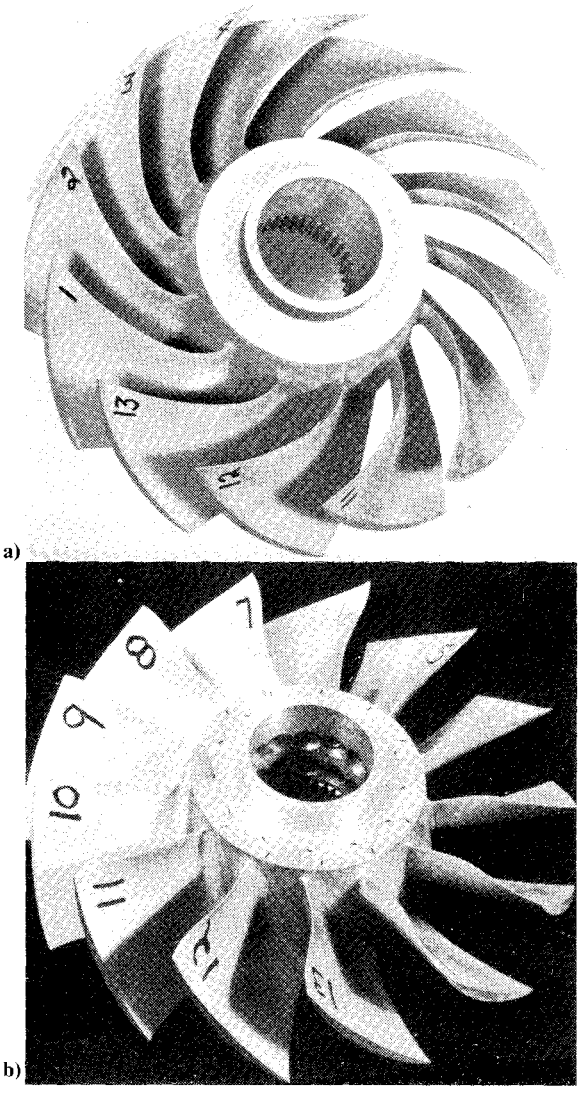

Fig. 5 Design I (a) skewed and (b) radial rotors.

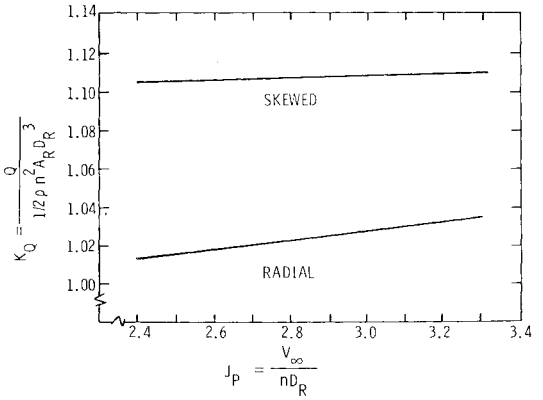

Fig. 6 Design I rotor torque coefficient as a function of advance ratio.

which is the preferred form of the radial equilibrium equation for computational purposes. The flowfield is, of course, also governed by the energy equation and the principles of conservation of angular momentum and mass (the continuity condition). For pump design applications this means that the total pressure is constant along a streamline in the absence of any losses or scheduled energy increases such as the rotor head increase. The term representing angular momentum $R \cdot V_\theta$ is also constant along a streamline in the absence of any induced change of V_θ. The term $(\sin\phi/V_M)(\partial V_M/\partial M)$ can be obtained from the continuity equation for an axially symmetric flow in cylindrical coordinates:

$$\frac{\sin\phi}{V_M}\frac{\partial V_M}{\partial M} = -\left[\frac{R}{R_C\cos\phi} + I\right]\frac{\sin^2\phi}{R} - \frac{\partial\phi}{\partial R}\tan\phi \qquad (11)$$

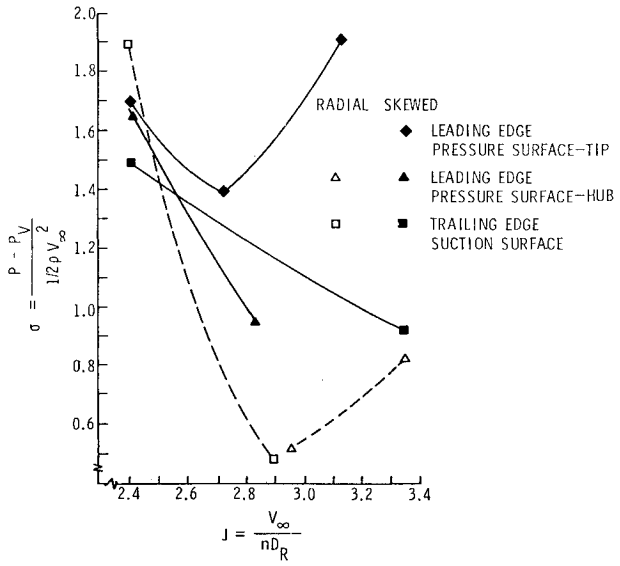

Fig. 7 Design I cavitation index as a function of advance ratio.

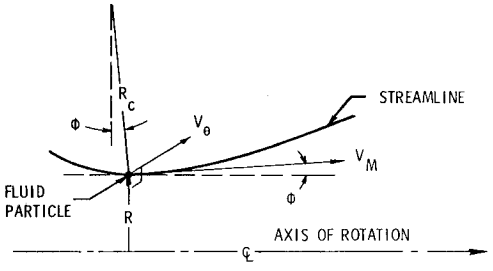

Fig. 8 Description of axially symmetric meridional flow.

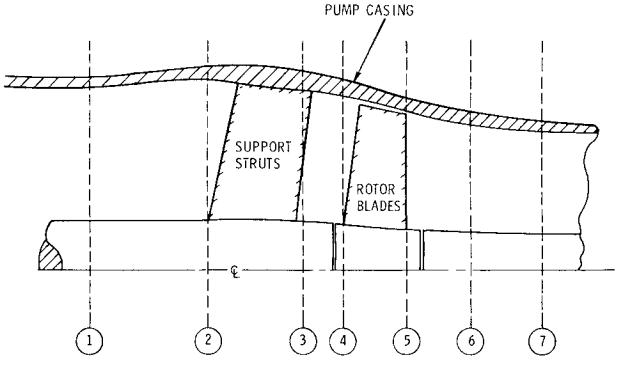

Fig. 9 Streamline curvature method computation stations.

For a typical pump design application such as that shown in Fig. 9 the radial distributions of pressures and velocities at the rotor inlet and exit planes (computing stations 4 and 5) are desired. In applying the SCM it is assumed that the radial distribution of velocities and pressures at station 1, the duct geometry, and the rotor pressure rise can be specified. The total pressure rise through the rotor, ΔP_T, permits a first approximation of the V_θ distribution at the rotor exit plane using Euler's pump equation. Assuming that the rotor inlet flow has no V_θ component

$$\bar{V}_{\theta_5} = \frac{\Delta P_T}{\rho U_5} = \frac{\Delta P_T \cdot J}{\pi\rho(\bar{R}/R_R)V_\infty} \qquad (12)$$

where U_5 has been expressed in terms of the design advance ratio J.

Equation (12) permits the calculation of an average value of $\bar{V}_{\theta_5}$. In practice, a radial variation of V_{θ_5} must be assumed which has the same integrated effect as $\bar{V}_{\theta_5}$.

In computerized SCM applications all radial distributions of flow parameters and streamline patterns are specified by differentiable spline curves.[5] Once the number and location of the computing stations and the number of streamlines are chosen, computations begin by making a first approximation of the streamline pattern on a continuity basis.

From the input V_θ profiles at stations 1 and 5, the angular momentum is defined as a function of radial position, and spline curves are passed through the resulting distributions. The angular momentum distributions for the intermediate stations are determined as a part of the solution and are governed by the conservation of angular momentum.

A spline curve is passed through the radial P_T distribution at station 1. In the absence of inlet losses, the value of P_T for

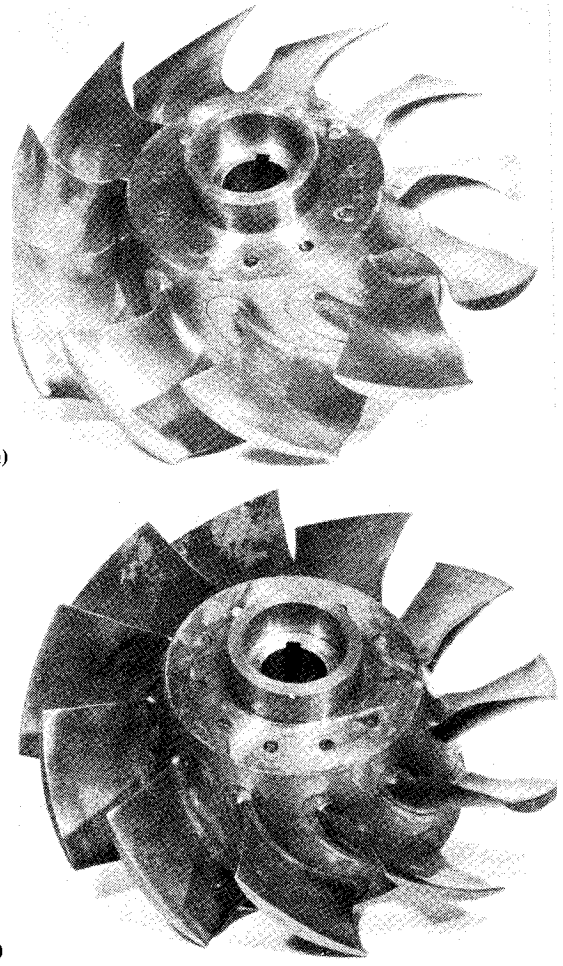

Fig. 10 Design II (a) skewed and (b) radial rotors

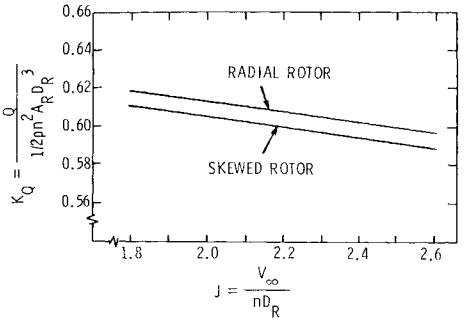

Fig. 11 Design II rotor torque coefficient as a function of advance ratio.

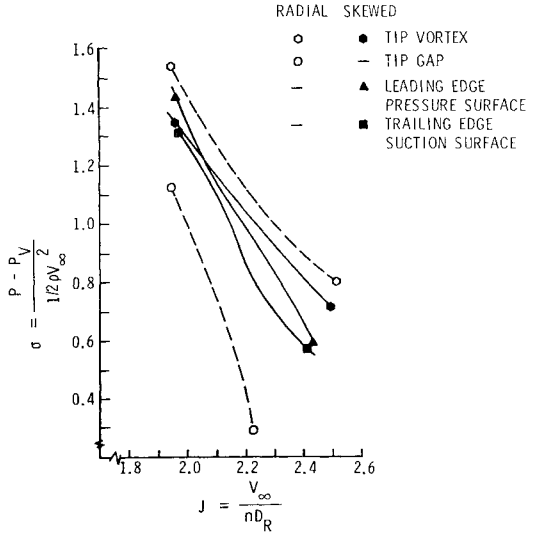

Fig. 12 Design II cavitation index as a function of advance ratio.

a given streamline is specified as a constant along the streamline from the reference station to the casing inlet where P_I is reduced by a radially constant percentage of the reference dynamic pressure for the particular streamline. These new values of P_I for a given streamline are specified as a constant to the leading edge of the rotor. At the rotor exit plane, the radial distribution of total pressure increase is calculated from the design V_θ distribution using Euler's pump equation and is specified as a function of radial distance by a spline curve. Secondary flow losses at the rotor exit plane are included from experimentally derived loss distributions. For a particular streamline, the new P_T value is the sum of the upstream value plus the net increment in P_T computed for that streamline at the rotor exit and is specified as a constant for the remaining axial stations.

From the spline curves of the approximated streamline pattern the necessary geometric properties of the flowfield—in particular the values of the radius of curvature R_C, the local angle of inclination of the streamlines with respect to the centerline ϕ, and $\partial\phi/\partial R$—can be calculated.

The streamline locations at station 1 are known from the reference velocity profile. The streamline locations at the other stations are determined on a station-by-station basis. A value of V_M is assumed at the midstreamline and, from the relevant spline curves, Eq. (11) and (10) can be evaluated to yield $\partial V_M/\partial R$ at the midstreamline. This value permits the computation of V_M at the two adjacent streamlines. This process is repeated across the duct until a V_M vs R profile is established. This profile is integrated to determine the associated C_m' value. The midstreamline value of V_M is adjusted and the computations are repeated until the resulting C_m' agrees with the design value. New streamline patterns are

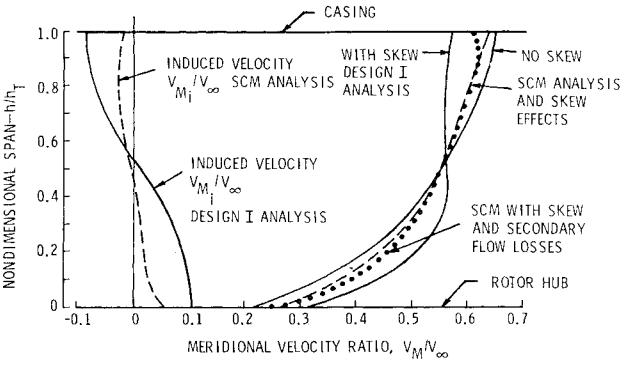

Fig. 13 Comparison of design I and SCM rotor inlet velocity ratio.

derived from the computed V_M profile. Horlock[6] has shown that it is frequently necessary to introduce a relaxation factor, η, in the adjustment to the calculated streamline spacing to assure the ultimate convergence of the solution. Thus, the new streamline locations at a particular station are adjusted to

$$R_{k+1} = \eta R_{k-1} + (1-\eta) R_k \tag{13}$$

Typically, $\eta \approx 0.8$.

This process of determining a new V_M profile and streamline spacing is repeated for all stations. Spline curves are developed to define the new streamline shapes. The entire process is repeated until the difference in streamline location for two successive passes through the program is within a specified limit for all streamlines at all stations. When this stable condition is reached, the program has defined the final solution.

The previously discussed version of the SCM is applicable only to axisymmetric turbomachine flows for the regions outside of the blade rows. To design skewed blading, the flow effects within the blade row must be involved. A first approach to an SCM solution to this problem is discussed by Treaster[7] and is summarized here. When heat addition and compressibility effects are neglected, the radial equilibrium equation for application within blade rows[2] has the following form:

$$\frac{1}{\rho}\frac{\partial P}{\partial R} = \frac{V_\theta^2}{R} + \frac{V_M^2}{R_C}\cos\phi - V_M\frac{\partial V_M}{\partial_M}\sin\phi + \frac{V_\ell}{\lambda}\tan\phi\frac{\mathrm{D}\lambda}{\mathrm{D}Z} + F_R \tag{14}$$

Equation (14) differs from Eq. (8) by the presence of the last two terms on the right-hand side. The first of these terms is a function of blade blockage, whereas the F_R term depends, in part, on the blade skew. The effective area coefficient is

$$\lambda = N/2\pi(\theta_s - \theta_p) \tag{15}$$

For the thin and approximately parallel blade sections used in this application

$$\frac{\mathrm{D}\lambda}{\mathrm{D}Z} \cong 0.0 \tag{16}$$

and the first of the new terms is omitted from the analysis. The second term, F_R, is the radial component of the body force which can be expressed as

$$F_R = \frac{\Delta P \tan\psi}{\rho R(\theta_s - \theta_p)} = \frac{N\Delta P \tan\psi}{2\pi\rho\lambda R} \tag{17}$$

where ΔP is the static pressure difference between the blades pressure and suction surfaces. When Eq. (17) is combined with Eq. (14) the "skewed" version of the radial equilibrium

equation for computation within blade rows results

$$\frac{\partial V_M}{\partial R} = \left[\frac{1}{\rho}\frac{\partial P_T}{\partial R} - \frac{V_\theta}{R}\frac{\partial (RV_\theta)}{\partial R} - F_R\right]\frac{1}{V_M}$$

$$-\left[\frac{\cos\phi}{R_c} - \frac{\sin\phi}{V_M}\cdot\frac{\partial V_M}{\partial_M}\right]V_M \qquad (18)$$

Thus, for the SCM analysis of an axisymmetric flowfield in which skewed blades are operating, Eq. (10) is applied to the region exterior to the blade rows and Eq. (18) is used within the blade rows. To avoid SCM convergence problems inherent in the use of closely spaced (high aspect ratio) computing stations, only one "skew" station was used within the blade row. The effects of the skewed blading on the neighboring stations are affected by the shifting of the spline curves representing the streamline pattern and the accompanying redistribution of the meridional velocity and static pressure profiles.

The parameters required to evaluate F_R and the nongeometric terms in Eq. (18) are computed from the typical blade section design parameters in Ref. 7 and are supplied to the SCM computer program via data statements. Once convergence of either the skewed or nonskewed version of the SCM has been achieved, all required velocity and pressure data at the rotor inlet and exit planes are available for the final blade section design.

In the case of the pump design II, both radial and skewed bladed rotors were designed using the streamline curvature method and included the effects of both inlet and secondary flow energy (total pressure) losses. The effects of blade skew were included as required. The blades were computer-lofted using spline curves[5] and fabricated on a three-axis numerically controlled milling machine. The resulting pump rotor configurations can be seen in Fig. (10).

Experimental Evaluation of Pump Design II

The design II skewed bladed pump rotor was subjected to a test program similar to that conducted for the design I skewed bladed pump. The K_Q vs J data are presented in Fig. 11. Again, the radial rotor was evaluated to provide performance comparisons. The data indicate that the skewed bladed rotor required ~1% less torque than the corresponding radial bladed rotor design. However, this is within the experimental accuracy; thus the torque requirements of the two rotors are essentially equal.

The cavitation characteristics of the two design II rotors are shown in Fig. 12. Here the skewed rotor has exhibited better cavitation resistance than the radial rotor, although both rotors are basically controlled by tip vortex cavitation.

In summary, these experimental data indicated that the design II skewed bladed pump rotor met or exceeded the design performance goals.

Reanalysis of the Design I Pump by Streamline Curvature Methods

The design I flowfield was reanalyzed using the SCM computer program. The computed data are shown in Fig. 13 along with original design I data from Fig. 3. The dashed curve shows the effect of skew on this design as specified by the SCM analysis. This figure shows how the design I procedure overestimated the induced effects of blade skew. The individual data points indicate the additional modification of the meridional velocity ratio when secondary flow losses are also considered.

The original test data for rotor design I and this reanalysis indicate that, in all probability, the design I rotor was operating at negative incidence angles over the outboard half of the blade span. This would make those blade sections prone to pressure surface cavitation, as observed. However, the inboard sections were operating at positive incidence angles and would therefore add increased turning to the flow. There is also evidence from the cavitation data that the blade may have been subject to flow separation. Both of these factors could have contributed to the higher torque values measured with the design I skewed rotor.

Conclusions

By incorporating secondary flow losses and one internal computing station within the rotor blade to simulate the skew effect, a pump rotor, design II, was designed which satisfied specified performance goals. The design I rotor failed to meet its design objectives, but when the flowfield was reanalyzed by streamline curvature methods the inadequacies in the original design procedure were illuminated. It should be made clear that these rotor design approaches were separated by more than 12 years in time. During this interval turbomachinery technology advanced and computer-adapted procedures were developed that replaced the laborious and less accurate hand computations and lofting of blade surfaces.

References

[1] Wislicenus, G. F., *Fluid Mechanics of Turbomachinery*, Vol. II, Dover Publications, New York, 1965, pp. 646-714.

[2] Smith, L. H., Traugott, S. C., and Wislicenus, G. F., "A Practical Solution of Three-Dimensional Flow Problem of Axial-Flow Turbomachinery," *Transactions of ASME*, Vol. 75, July 1953, pp. 789-803.

[3] Novak, R. A., "Streamline Curvature Computing Procedures for Fluid Flow Problems," ASME Paper 66-WA/GT-3, Nov. 1966.

[4] Treaster, A. L., "Computerized Application of the Streamline Curvature Method to the Indirect Axisymmetric Turbomachine Problem," Applied Research Laboratory, TM 514.2491-16, Oct. 1969.

[5] Davis, R. F., "Spline Curve Fit Functions, Their Derivation and Use," Ordnance Research Laboratory, TM 512.3531-02, July 1968.

[6] Horlock, J. H., *Axial Flow Compressors*, Butterworth Scientific Publications, London, 1968.

[7] Treaster, A. L., "PRESKEW: Preliminary Skew Analysis Program," Applied Research Laboratory TM 77-62, March 1977.

[8] McBride, M. W., "Refinement of the Mean Streamline Method of Blade Section Design," *Transactions of ASME, Journal of Fluids Engineering*, Vol. 99, Sept. 1977, pp. 561-566.

[9] Davis, R. F., "Marine Propulsor Blade Lofting," *Proceedings of American Ordnance Association*, May 1971.